center of the primary winding to complete the magnetic path when the coupler is inserted into the vehicle inlet. The disassembled transformer components are shown in Figure 14.17(b).

An off-vehicle high-frequency power converter feeds the cable, coupler, vehicle-charging inlet, and battery load. The EV user physically inserts the coupler into the vehicle inlet where the high-frequency power is transformer-coupled, rectified, and fed to the battery. The technology was researched and productized at levels ranging from a few kilowatts to tens of kilowatts, with a high-power demonstration at 120 kW [3–6]. A recommended practice for inductive charging of EVs, SAE J1773, was published by the SAE. The specifications, as outlined in SAE J1773, for the coupler and vehicle inlet characteristics were to be considered when selecting a driving topology. Among the most critical parameters are the frequency range, the low magnetizing inductance, the high leakage inductance, and the significant discrete parallel capacitance. The off-vehicle EV1 charge module features a frequency-controlled series-resonant converter. Driving the SAE J1773 vehicle interface with the series-resonant converter results in a four-element topology with many desirable features. This resonant topology is discussed in detail in Chapter 12, Section 12.4.

14.5.5.2 Wireless

The inductive charging system developed by GM is no longer used as the market shifted to conductive standards. However, new wireless charging standards are being developed for EVs as wireless charging is once again being viewed positively for developing the EV market. An interesting application of wireless charging is driverless vehicles, as charging can be facilitated without human actions. Recent interest in wireless charging has been in loosely coupled transformer systems. The principles are similar to the inductive coupling just described, with the difference that the transformer primary and secondary assemblies are spaced many centimeters apart and have relatively greater leakage inductances.

Worldwide standards are being developed. SAE J2954 is the SAE standard. The technology is also dependant on the types of resonant circuits discussed in Chapter 12 for application to inductive coupling. Additional safety issues must be addressed, such as the effects of radiation on humans and animals and the presence of metal objects in the magnetic fields.

14.6 The Boost Converter for Power Factor Correction

The front-end of the charger is a power-factor-correction stage utilizing a boost converter. An example of an automotive charger is shown in Figure 14.18. The charger features an interleaved boost and so has two boost inductors, shown with an L. The input (IP) power first flows through the EMI filter (EMI) and is then rectified (R) and boosted (Q+D, L). The charger requires a significant electrolytic bulk capacitor stage (C) in order to filter the 50/60 Hz ripple. The full-bridge converter stage features the power transformers (Xo), the full-bridge switches and diodes (Qo+Do), the output rectifier (Ro), the output inductor (Lo), and output filtering (EMIo). The full-bridge converter is discussed in depth in Chapter 12. The focus of this section is on the boost PFC, as shown in Figure 14.19(a).

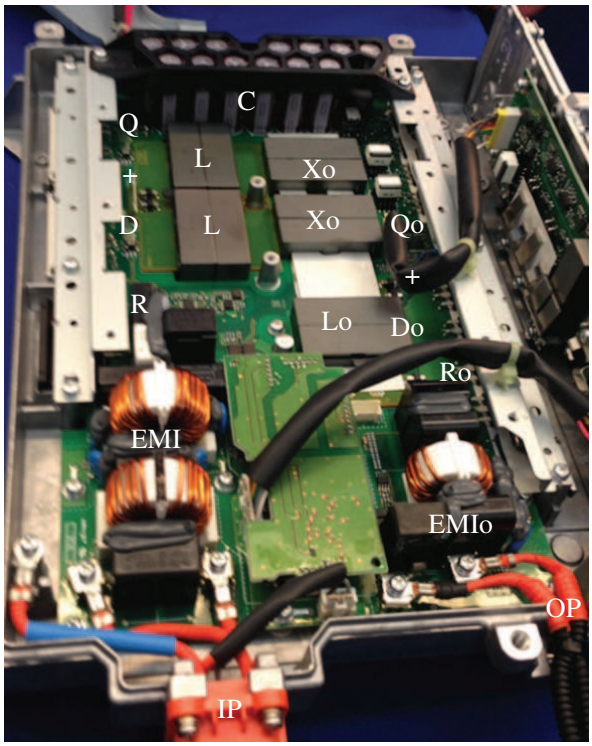

Figure 14.18 Automotive EV charger.

14.6.1 The Boost PFC Power Stage

The input current is controlled to be in phase with the supply voltage. This is achieved by using two control loops: an inner current loop and an outer voltage loop. The converter typically achieves very high power factors with values greater than 0.99 being reasonable at full load [7–9].

The ac voltages and currents are rectified by the input bridge. Let the ac voltage be

$$v_{ac}(\theta) = \sqrt{2}V_{ph}\cos\theta \tag{14.3}$$

Using the boost PFC, the ac current is controlled to be in phase with the voltage:

$$i_{ac}(\theta) = \sqrt{2}I_{ph}\cos\theta \tag{14.4}$$

The voltage v_{RB} and current i_{RB} from the rectifier bridge are

$$v_{RB}(\theta) = \sqrt{2}V_{ph}|\cos\theta| \tag{14.5}$$

$$i_{RB}(\theta) = \sqrt{2}I_{ph}|\cos\theta| \tag{14.6}$$

The boost converter controls the inductor current i_L to be in phase with the rectified input voltage v_{RB}, as shown in Figure 14.19(b) The inductor current carries the PWM ripple current as shown in Figure 14.19(c).

The capacitor at the output of the rectifier C_R is there to filter the PWM ripple current of the inductor.

The size of the dc link capacitor in a PFC boost converter is based on three factors: (1) the desired hold-up time of the capacitors, (2) the current rating and aging of the electrolytic capacitors, and (3) the low-frequency voltage ripple. All three factors must

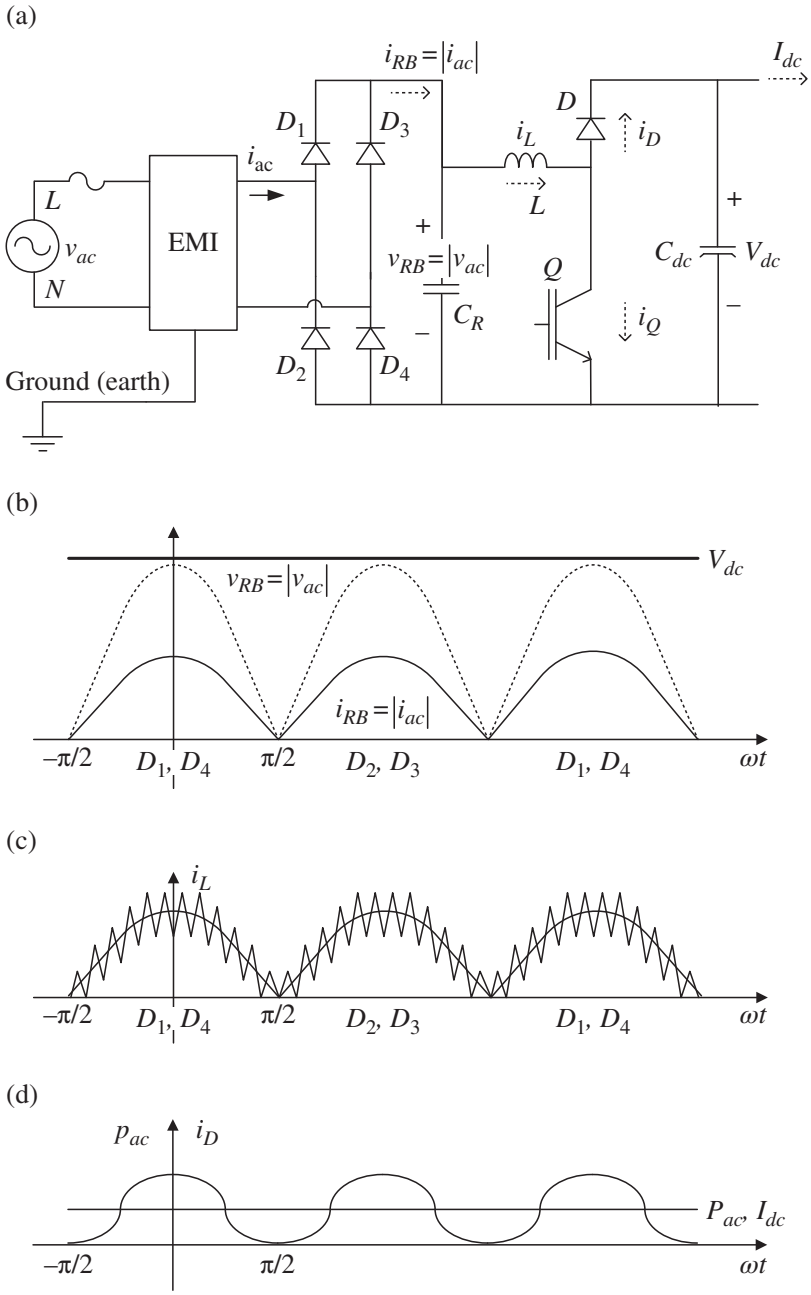

Figure 14.19 Boost PFC and waveforms.

be considered when designing the power and control stages. The dc link capacitor is usually a bank of bulky electrolytic capacitors, which are sized to minimize the low-frequency voltage ripple due to the high second harmonic of the dc link current.

The EMI stage provides common-mode and differential-mode EMI filtering in order to meet the applicable EMC standards [10–13]. It is common for EMI stages to comprise 10% to 20 % of the volume of the charger or of the generic power converter.

The power pulled from the ac source p_{ac} has a pulsing sine^2 characteristic given by

$$p_{ac}(\theta) = v_{ac}(\theta) \times i_{ac}(\theta) = \sqrt{2}V_{ph}\cos\theta \times \sqrt{2}I_{ph}\cos\theta = 2V_{ph}I_{ph}\cos^2\theta \tag{14.7}$$

with an average power P_{ac} given by

$$P_{ac} = V_{ph} I_{ph} \tag{14.8}$$

The characteristic of the power is as shown in Figure 14.19(d). The input power pulses from zero to twice the average power with a sine-squared (sine^2) characteristic.

If we consider the low-frequency characteristic of the diode current, then the diode current also has a low-frequency sine^2 characteristic at twice the line frequency as shown in Figure 14.19(d). Neglecting PWM, the low-frequency dc link power is given by

$$p_D(\theta) = V_{dc} \times i_D(\theta) \tag{14.9}$$

If we ignore the rectifier and boost power loss, the instantaneous dc link power p_D equals the input power p_{ac}:

$$p_D(\theta) = p_{ac}(\theta) \tag{14.10}$$

and so

$$i_D(\theta) = \frac{p_{ac}(\theta)}{V_{dc}} = \frac{2V_{ph}I_{ph}}{V_{dc}} \cos^2\theta \tag{14.11}$$

Thus, the boost diode has a similar low-frequency sine^2 current characteristic, with power pulses from zero to twice the average power as shown in Figure 14.19(d). The average of the diode current equals the dc link current I_{dc} and is given by

$$I_{dc} = \frac{P_{ac}}{V_{dc}} = \frac{V_{ph}I_{ph}}{V_{dc}} \tag{14.12}$$

This low-frequency current at twice the line frequency is typically filtered by the dc link capacitor C_{dc}. It is also an option in battery chargers to have the sine^2 current flow into the battery, significantly reducing the requirement for the dc link capacitor [14]. However, **sine^2 charging**, as it is known, increases the ripple current flowing into the battery.

14.6.2 Sizing the Boost Inductor

The boost inductor is sized in order to limit the ripple current and reduce harmonics and EMI. From the analysis of the CCM boost in Chapter 11 Section 11.4.1, the duty cycle of the boost switch is given by

$$d(\theta) = 1 - \frac{v_{RB}(\theta)}{V_{dc}} = 1 - \frac{\sqrt{2}V_{ph}|\cos\theta|}{V_{dc}} \tag{14.13}$$

The peak-to-peak ripple current is

$$\Delta I_{L(p-p)}(\theta) = \frac{\sqrt{2}V_{ph}|\cos\theta|}{f_s L} d(\theta) = \frac{\sqrt{2}V_{ph}}{f_s L}\left(|\cos\theta| - \frac{\sqrt{2}V_{ph}\cos^2\theta}{V_{dc}}\right) \tag{14.14}$$

and so the ripple current magnitude clearly varies with duty cycle.

14.6.2.1 Example: Sizing the Inductor

A 3.3 kW PFC boost is designed for a nominal input voltage of 230 V, 50/60 Hz with an input voltage ranging from a low line of 180 V to a high line of 265 V. Determine the value of the boost inductor and the peak inductor current if the switching frequency is 100 kHz

and the peak-to-peak ripple ratio is 20% of the peak low-frequency current at the peak of the nominal input voltage. The dc link voltage is 380 V. Ignore the power loss.

Solution:

The rms input current is

$$I_{ph} = \frac{P}{V_{ph}} = \frac{3300}{230}\text{A} = 14.35\,\text{A}$$

The peak of the input current is

$$I_{ph(peak)} = \sqrt{2}I_{ph} = \sqrt{2} \times 14.35\,\text{A} = 20.29\,\text{A}$$

The peak-to-peak ripple current at the peak of the input voltage is

$$\Delta I_{L(p-p)} = r_i I_{ph(peak)} = 0.2 \times 20.29\,\text{A} = 4.06\,\text{A}$$

The duty cycle at the peak of the input voltage is

$$d(0) = 1 - \frac{\sqrt{2}V_{ph}|\cos 0|}{V_{dc}} = 1 - \frac{\sqrt{2}V_{ph}}{V_{dc}} = 1 - \frac{\sqrt{2} \times 230}{380} = 0.1440$$

The required inductance is determined by rearranging Equation (14.14):

$$L = \frac{\sqrt{2}V_{ph}|\cos 0|}{f\,\Delta I_{L(p-p)}(0)}d(0) = \frac{\sqrt{2} \times 230}{100 \times 10^3 \times 4.06} \times 0.144\,\text{H} = 115\,\mu\text{H}$$

The peak current in the inductor is the sum of the peak of the line current and half of the peak-to-peak ripple:

$$I_{L(peak)} = I_{ph(peak)} + \frac{\Delta I_{L(p-p)}}{2} \tag{14.15}$$

In this case:

$$I_{L(peak)} = I_{ph(peak)} + \frac{\Delta I_{L(p-p)}}{2} = 20.29\text{A} + \frac{4.06}{2}\text{A} = 22.32\,\text{A}$$

Once the peak and rms currents are known, the inductor can be sized as covered in Chapter 16, Section 16.3.7, using the area-product method. The rms input current can be used as a reasonable approximation for the rms inductor current.

14.6.3 Average Currents in the Rectifier

The input rectifier diodes alternately conduct. Diodes D_1 and D_4 conduct during the positive half cycle, while diodes D_2 and D_3 conduct during the negative half cycle.

The average current in the rectifier diodes $I_{R(dc)}$ for a half cycle is

$$I_{R(dc)} = I_{D1(dc)} = I_{D4(dc)} = \frac{1}{2\pi}\int_{-\frac{\pi}{2}}^{\frac{\pi}{2}} i_{RB}(\theta)d\theta = \frac{1}{2\pi}\int_{-\frac{\pi}{2}}^{\frac{\pi}{2}} \sqrt{2}I_{ph}\cos\theta d\theta = \frac{I_{ph}}{\sqrt{2}\pi}\int_{-\frac{\pi}{2}}^{\frac{\pi}{2}} \cos\theta d\theta = \frac{\sqrt{2}}{\pi}I_{ph} \tag{14.16}$$

The rms current in the rectifier diodes $I_{R(rms)}$ for a half cycle is

$$I_{R(rms)} = I_{D1(rms)} = I_{D4(rms)} = \sqrt{\frac{1}{2\pi}\int_{-\frac{\pi}{2}}^{\frac{\pi}{2}} (i_{RB}(\theta))^2 d\theta} = \sqrt{\frac{1}{2\pi}\int_{-\frac{\pi}{2}}^{\frac{\pi}{2}} \left(\sqrt{2}I_{ph}\cos\theta\right)^2 d\theta} = \frac{1}{\sqrt{2}}I_{ph} \tag{14.17}$$

The values of the dc and rms currents in diodes D_2 and D_3 are the same as in diodes D_1 and D_4.

14.6.3.1 Example: Input Rectifier Power Loss

Determine the power loss in the input rectifier stage of the earlier example if each rectifier has the following parameters: V_{f0} =0.8 V and r_f = 10 mΩ.

Solution:

The average current in the rectifier diodes for a half cycle is

$$I_{R(dc)} = \frac{\sqrt{2}}{\pi}I_{ph} = \frac{\sqrt{2}}{\pi} \times 14.35\,\text{A} = 6.46\,\text{A}$$

The rms current in the rectifier diodes for a half cycle is

$$I_{R(rms)} = \frac{1}{\sqrt{2}}I_{ph} = \frac{1}{\sqrt{2}} \times 14.35\,\text{A} = 10.15\,\text{A}$$

Per the section on semiconductor losses in Chapter 11, Section 11.5, the conduction loss per rectifier diode is

$$P_{R(cond)} = V_{f0}I_{R(dc)} + r_f I_{R(rms)}^2 \tag{14.18}$$

In this case:

$$P_{R(cond)} = V_{f0}I_{R(dc)} + r_f I_{R(rms)}^2 = 0.8 \times 6.46\,\text{W} + 0.01 \times 10.15^2\,\text{W} = 6.2\,\text{W}$$

The loss in the rectifier bridge P_{RB} is four times the loss in a single rectifier diode:

$$P_{RB} = 4 \times P_{R(\text{cond})} \tag{14.19}$$

For this example:

$$P_{RB} = 4 \times P_{R(\text{cond})} = 4 \times 6.2\,\text{W} = 24.8\,\text{W}$$

14.6.4 Switch and Diode Average Currents

The duty cycle of the boost switch is given by Equation (14.13).

The low-frequency time-averaged current in the switch can be approximated by

$$i_Q(\theta) = d(\theta) \times |i_{ac}(\theta)| \tag{14.20}$$

Substituting in Equation (14.4) and Equation (14.13) yields:

$$i_Q(\theta) = \left(1 - \frac{\sqrt{2}V_{ph}|\cos\theta|}{V_{dc}}\right) \times \sqrt{2}I_{ph}\cos\theta \tag{14.21}$$

or

$$i_Q(\theta) = \sqrt{2} I_{ph} \cos\theta - \frac{2 V_{ph} I_{ph} \cos^2\theta}{V_{dc}} \tag{14.22}$$

The average current in the switch is given by

$$I_{Q(dc)} = \frac{1}{\pi} \int_{-\frac{\pi}{2}}^{\frac{\pi}{2}} i_Q(\theta) d\theta \tag{14.23}$$

Substituting Equation (14.22) into Equation (14.23) yields

$$I_{Q(dc)} = \frac{I_{ph}}{\pi} \int_{-\frac{\pi}{2}}^{\frac{\pi}{2}} \left(\sqrt{2}\cos\theta - \frac{2 V_{ph} \cos^2\theta}{V_{dc}} \right) d\theta \tag{14.24}$$

which simplifies to

$$I_{Q(dc)} = I_{ph} \left(\frac{2\sqrt{2}}{\pi} - \frac{V_{ph}}{V_{dc}} \right) \tag{14.25}$$

since

$$\int_{-\frac{\pi}{2}}^{\frac{\pi}{2}} \cos\theta d\theta = 2 \quad \text{and} \quad \int_{-\frac{\pi}{2}}^{\frac{\pi}{2}} \cos^2\theta d\theta = \frac{\pi}{2} \tag{14.26}$$

Similarly, the low-frequency time-averaged current in the boost diode is given by

$$i_D(\theta) = (1 - d(\theta)) \times |i_{ac}(\theta)| \tag{14.27}$$

which expands to

$$i_D(\theta) = \left(\frac{\sqrt{2} V_{ph} |\cos\theta|}{V_{dc}} \right) \times \sqrt{2} I_{ph} \cos\theta \tag{14.28}$$

The diode conducts the current for half the period, and the average current is

$$I_{D(dc)} = \frac{1}{\pi} \int_{-\frac{\pi}{2}}^{\frac{\pi}{2}} i_D(\theta) d\theta = \frac{1}{\pi} \int_{-\frac{\pi}{2}}^{\frac{\pi}{2}} \frac{2 V_{ph} I_{ph} \cos^2\theta}{V_{dc}} d\theta = \frac{2 V_{ph} I_{ph}}{\pi V_{dc}} \int_{-\frac{\pi}{2}}^{\frac{\pi}{2}} \cos^2\theta d\theta \tag{14.29}$$

which simplifies to

$$I_{D(dc)} = \frac{V_{ph} I_{ph}}{V_{dc}} \tag{14.30}$$

14.6.5 Switch, Diode, and Capacitor RMS Currents

The rms current in the boost switch can be approximated by

$$I_{Q(rms)} = \sqrt{\frac{1}{\pi}\int_{-\frac{\pi}{2}}^{\frac{\pi}{2}} d(\theta)(i_{ac}(\theta))^2 d\theta} \tag{14.31}$$

Substituting in Equation (14.4) and Equation (14.13) gives

$$I_{Q(rms)} = \sqrt{\frac{1}{\pi}\int_{-\frac{\pi}{2}}^{\frac{\pi}{2}} \left(1 - \frac{\sqrt{2}V_{ph}|\cos\theta|}{V_{dc}}\right) \times \left(\sqrt{2}I_{ph}\cos\theta\right)^2 d\theta} \tag{14.32}$$

which simplifies to

$$I_{Q(rms)} = I_{ph}\sqrt{\frac{1}{\pi}\int_{-\frac{\pi}{2}}^{\frac{\pi}{2}} \left(2\cos^2\theta - \frac{2\sqrt{2}V_{ph}|\cos\theta|\cos^2\theta}{V_{dc}}\right) d\theta} \tag{14.33}$$

Since

$$\int_{-\frac{\pi}{2}}^{\frac{\pi}{2}} |\cos\theta|\cos^2\theta d\theta = \frac{4}{3} \tag{14.34}$$

the rms current in the switch is given by

$$I_{Q(rms)} = I_{ph}\sqrt{1 - \frac{8\sqrt{2}V_{ph}}{3\pi V_{dc}}} \tag{14.35}$$

Similarly the rms current in the boost diode is given by

$$I_{D(rms)} = I_{ph}\sqrt{\frac{8\sqrt{2}V_{ph}}{3\pi V_{dc}}} \tag{14.36}$$

The rms current in the high-voltage dc link capacitor $I_{Cdc(rms)}$ is simply given by

$$\begin{aligned} I_{Cdc(rms)} &= \sqrt{I_{D(rms)}{}^2 - I_{D(dc)}{}^2} \\ &= I_{ph}\sqrt{\frac{8\sqrt{2}V_{ph}}{3\pi V_{dc}} - \frac{V_{ph}{}^2}{V_{dc}{}^2}} \end{aligned} \tag{14.37}$$

14.6.6 Power Semiconductors for Charging

While the silicon IGBT and the silicon diode are dominant for low-to-medium switching frequencies, the silicon MOSFET is typically preferred at higher switching frequencies

for low- and medium-range voltages (<600 V). The conduction loss in the MOSFET can be simply modeled by the **drain-source on-resistance**, typically designated $\boldsymbol{R_{DS(on)}}$. The maximum $R_{DS(on)}$ is usually specified for the component. A characteristic of the power MOSFET is that the on-resistance typically doubles between 25°C and 120°C.

The MOSFET conduction loss is given by

$$P_{Q(\text{cond})} = R_{DS(on)} I_{Q(rms)}{}^2 \tag{14.38}$$

As $R_{DS(on)}$ increases with an index somewhere between the square and cube of the device voltage rating, the silicon MOSFET cannot compete with the silicon IGBT for higher voltages. However, the MOSFET is a competitive device for a high-frequency PFC boost.

A significant source of power loss for the switching pole is the reverse recovery loss of the boost diode. This loss can be eliminated by employing the more expensive wide-band-gap **silicon-carbide** (**SiC**) **Schottky diode**, which has no reverse recovery loss.

The average current in the diode and switch when switched is

$$I_{Q(sw,avg)} = I_{D(sw,avg)} = \frac{2\sqrt{2}}{\pi} I_{ph} \tag{14.39}$$

Similar to the IGBT in Chapter 11, Section 11.5.1.3, the MOSFET switching power losses remain

$$P_{Q(sw)} = f_s \left(E_{on} + E_{off}\right) \frac{V_{dc}}{V_{test}} \tag{14.40}$$

It is assumed for simplicity that the switching loss for the SiC diode is zero.

In the final part of this section, the losses are estimated for the semiconductor switches in the boost PFC.

14.6.6.1 Example: Silicon MOSFET and SiC Diode Power Losses

The PFC boost converter of the examples used in this chapter features a representative silicon MOSFET and a SiC diode, nominally the part MKE 11R600DCGFC from manufacturer IXYS [15].

The nominal maximum $R_{DS(on)}$ of the device is specified as 0.165 Ω at 25°C, but increases to about 0.375 Ω at 125°C as shown in Figure 14.20(a).

The diode conduction drops are shown in Figure 14.20(b) and can be modeled by V_{f0} = 0.8 V and r_f = 8.8 mΩ at 125°C.

The MOSFET switching losses are shown in Figure 14.21. The diode switching losses are ignored.

Determine the MOSFET and diode power losses, assuming junction temperatures of 125°C.

Solution:

The switch rms current is

$$I_{Q(rms)} = I_{ph}\sqrt{1 - \frac{8\sqrt{2}V_{ph}}{3\pi V_{dc}}} = 14.35 \times \sqrt{1 - \frac{8\sqrt{2} \times 230}{3\pi \times 380}}\,\text{A} = 7.504\,\text{A}$$

The MOSFET conduction loss is

$$P_{Q(\text{cond})} = R_{DS(on)} I_{Q(rms)}{}^2 = 0.375 \times 7.504^2\,\text{W} = 21.1\,\text{W}$$

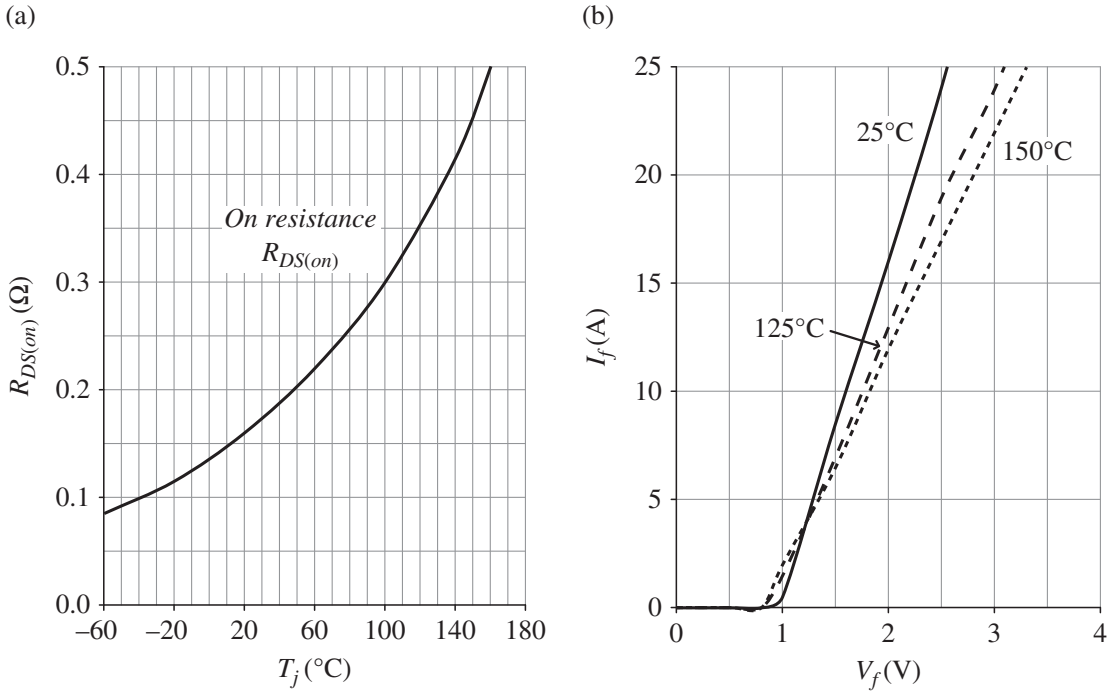

Figure 14.20 Representative 600 V, 15 A MOSFET and SiC diode conduction characteristics.

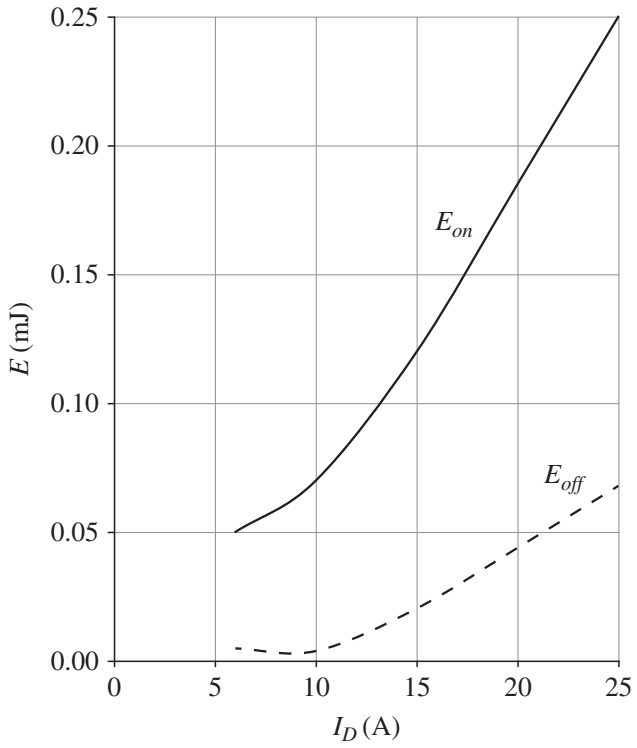

Figure 14.21 Representative 600 V, 15 A MOSFET (and SiC diode) turn-on and turn-off switching losses at 125°C and a test voltage of 380 V_{dc}.

The diode average and rms currents are

$$I_{D(dc)} = \frac{V_{ph}I_{ph}}{V_{dc}} = \frac{230 \times 14.35}{380}\text{A} = 8.69\,\text{A}$$

$$I_{D(rms)} = I_{ph}\sqrt{\frac{8\sqrt{2}V_{ph}}{3\pi V_{dc}}} = 14.35 \times \sqrt{\frac{8\sqrt{2} \times 230}{3\pi \times 380}}\text{A} = 12.23\,\text{A}$$

The diode conduction loss is

$$P_{D(\text{cond})} = V_{f0}I_{D(dc)} + r_f I_{D(rms)}{}^2 = 0.8 \times 8.69\,\text{W} + 0.0088 \times 12.23^2\,\text{W} = 8.3\,\text{W}$$

For a sinusoidal excitation, the average switching current in the switch and diode is

$$I_{Q(sw,avg)} = I_{D(sw,avg)} = \frac{2\sqrt{2}}{\pi}I_{ph} = \frac{2\sqrt{2}}{\pi}14.35\,\text{A} = 12.92\,\text{A}$$

The turn-on and turn-off power loss in the switch is

$$P_{Q(sw)} = f_s\left(E_{on} + E_{off}\right)\frac{V_{dc}}{V_{test}} = 100 \times 10^3\left(0.1 \times 10^{-3} + 0.013 \times 10^{-3}\right)\frac{380}{380}\text{W} = 11.3\,\text{W}$$

where E_{on} = 0.1 mJ and E_{off} = 0.013 mJ at 12.92 A from Figure 14.21.

The power losses in the switch and diode are

$$P_Q = P_{Q(cond)} + P_{Q(sw)} = 21.1\,\text{W} + 11.3\,\text{W} = 32.4\,\text{W}$$

and

$$P_D = P_{D(cond)} = 8.3\,\text{W}$$

14.6.6.2 Example: PFC Stage Losses

If the equivalent series resistance of the inductor is R_{cu} = 50 mΩ, and the combined auxiliary power and stray power loss P_{aux} is 15 W, determine the overall PFC converter power loss and efficiency.

Solution:

The inductor loss is

$$P_L = R_{cu}I_{ph}^2 = 0.05 \times 14.35^2\,\text{W} = 10.3\,\text{W}$$

The auxiliary and stray loss is

$$P_{aux} = 15\,\text{W}$$

The total loss is the sum of the losses in the inductor, the auxiliary circuits, the bridge rectifier, and the boost switch and diode:

$$P_{loss} = P_L + P_{aux} + P_{RB} + P_Q + P_D = 10.3\text{ W} + 15\text{ W} + 24.8\text{ W} + 32.4\text{ W} + 8.3\text{ W} = 90.8\text{ W}$$

The approximate efficiency is

$$\eta = \frac{P}{P + P_{loss}} \times 100\% = \frac{3300}{3300 + 90.8} \times 100\% = 97.3\%$$

References

1 *SAE Electric Vehicle and Plug in Hybrid Electric Vehicle Conductive Charge Coupler, SAE J-1772*, Society of Automotive Engineers.
2 *SAE Power Quality Requirements for Plug-In Electric Vehicle Chargers, SAE J-2894,* Society of Automotive Engineers.
3 J. G. Hayes, *Resonant Power Conversion Topologies for Inductive Charging of Electric Vehicle Batteries*, PhD Thesis, University College Cork, 1998.
4 *SAE Electric Vehicle Inductive Coupling Recommended Practice, SAE J-1773*, Society of Automotive Engineers, Draft, Feb. 1, 1995.
5 R. Severns, E. Yeow, G. Woody, J. Hall, and J. Hayes, "An ultra-compact transformer for a 100 W to 120 kW inductive coupler for electric vehicle battery charging," *IEEE Applied Power Electronics Conference*, pp. 32–38, 1996.
6 J. G. Hayes, N. O'Donovan, and M. G. Egan, "Inductance characterization of high-leakage transformers," *IEEE Applied Power Electronics Conference*, pp. 1150–1156, 2003.
7 N. Mohan, *Power Electronics A First Course*, Chapter 6, John Wiley & Sons, 2012.
8 S. Abdel-Rahman, F. Stuckler, and K. Siu, *PFC Boost Converter Design Guide 1200 W Design Example*, Infineon Application Note, 2016.
9 Texas Instruments, *UCC2817, UCC2818, UCC3817 and UCC3818 BiCMOS Power Factor Preregulator*, Unitrode Products from Texas Instruments, revised 2015.
10 M. Nave, *Power Line Filter Design for Switched-Mode Power Supplies*, Van Nostrand Reinhold, 1991.
11 H. W. Ott, *Electromagnetic Compatibility Engineering*, John Wiley & Sons, 2009.
12 P. Bardos, "Predicting the EMC performance of high-frequency inverters," *IEEE Applied Power Electronics Conference*, pp. 213–219, 2001.
13 M. Kacki, M. Rylko, J. G. Hayes, and C. R. Sullivan, "Magnetic material selection for EMI filters," *IEEE Energy Conversion Congress and Exposition*, 2017.
14 M. G. Egan, D. O'Sullivan, J. G. Hayes, M. Willers, and C. P. Henze, "Power-factor-corrected single-stage inductive charger for electric-vehicle batteries," *IEEE Transactions on Industrial Electronics*, 54 (2), pp. 1217–1226, April 2007.
15 Website of IXYS Corp., www.ixys.com.

Further Reading

1 N. Mohan, T. M. Undeland, and W. P. Robbins, *Power Electronics Converters, Applications and Design*, 3rd edition, John Wiley & Sons, 2003.
2 R. W. Erickson, *Fundamentals of Power Electronics*, Chapter 17, Kluwer Academic Publishers, 2000.
3 M. Yilmaz and P. T. Krein, "Review of battery charger topologies, charging power levels, and infrastructure for plug-in electric and hybrid vehicles," *IEEE Transactions on Power Electronics*, 28 (5), pp. 2151–2169, May 2013.
4 R. Ryan, J. G. Hayes, R. Morrison, and D. Hogan, "Digital control of an interleaved BCM boost PFC converter with fast transient response at low input voltage," *IEEE Energy Conversion Congress and Exposition*, 2017.